UAV Path Planning based on Road Extraction

Chang Liu[1] [a] and Tamás Szirányi[1,2] [b]

[1]*Department of Networked Systems and Services, Budapest University of Technology and Economics,*
Műegyetem rkp. 3, Budapest, Hungary
[2]*Machine Perception Research Laboratory of Institute for Computer Science and Control (SZTAKI),*
Kende u. 13-17, Budapest, Hungary

Keywords: Image Segmentation, Road Extraction, Weighted Path Planning, *A Star* Algorithm, UAV, SAR.

Abstract: With the development of science and technology, UAVs are increasingly being used and serving humans, especially in the wilderness environment, due to their portability and the ease with which they can reach places that are beyond human reach. In this paper, we present a technique for drones to help humans intelligently plan routes in a field environment. Our approach is firstly based on road extraction techniques in the field of image segmentation, using state-of-the-art *D-LinkNet* to extract roads from images captured by real-time UAVs. Secondly, the extracted road information is analyzed, the set of main roads and that of the secondary road are distinguished according to the width and the real-time road conditions on the ground, and different weights are assigned to them. Finally, the *A star* algorithm is used to calculate a route plan with weights based on the human-defined starting and ending points to obtain the optimal route. The results of our task are the simulations on publicly available datasets to show that the method works well to provide the optimal intelligent routes in real-time for people in the field.

1 INTRODUCTION

With the development of computer vision technology, drone vision technology is increasingly used in various fields of human life, providing convenience for human daily activity. For example, in agriculture, drones can help farmers to estimate the yield and size of citrus fruits (Apolo, 2020); in the field of medicine, the fleet of drones available for logistics to deliver medical items (Ghelichi, 2021); in the field of disaster relief, drones can detect fires (Moumgiakmas, 2021) and floods (Rizk, 2022), and so on. In the field of wilderness rescue, one of the biggest advantages of drones is their flexibility, as they can easily reach places that are inaccessible to humans, i.e. rescuers, making the use of GPU-equipped drone vision technology a viable option for rescue in difficult environments in the field, especially where there is no internet. The development of drone technology allows for endless possibilities in the future, but of course, we also have to take into account the performance of the GPU we are equipped with and

the battery life, among other things (Galkin, 2019), which are closely related. When it comes to the wilderness, which can be accompanied by poorly developed networks and roads that are not in good condition, or even roads that are not included in Google Maps (Ciepłuch, 2010), we consider the use of flexible drone vision technology to provide intelligent route planning for these people in the wilderness. In addition to its flexibility, the images captured by drones have a higher resolution than those captured by satellites and are more practical in people's daily lives, as they are still more accessible and on time to humans than satellites, and they can better serve people's lives. Based on our previous work (Liu, 2021), drones can interact well with humans in the wild and can recognize some hand gestures, and communicate more easily.

This work proposes a method for UAVs to plan intelligent routes in real-time for people in the wild field. The desired usage scenarios and the introduction diagram are shown in Figure 1. The method mainly extracts map images from the real-time video sequences captured by the UAV, converts

[a] https://orcid.org/0000-0001-6610-5348

[b] https://orcid.org/0000-0003-2989-0214

them into three-channel fixed resolution images through image processing techniques, these images are used as input for the road extraction process, outputs the road extraction results through *D-LinkNet* (Zhou, 2018), and finally gives different weights for intelligent route planning through road information analysis. Combining weather information with road information, it is important to assign weights to the proposed roads to help humans avoid roads in bad condition (e.g. muddy areas in the rain or snowy after snowing, or sandy after sand-storm) and choose roads in better condition. This is the starting point for assigning weights to different roads of specific conditions. Road information mainly includes road width, road surface material, and the environmental pollution covering the road surface (flood, mud, rubble), estimated from satellite hyperspectral data and the weather conditions. Generally speaking, large, spacious roads are in better condition than small, narrow roads on rainy days, and roads with asphalt surface material are in better condition than soil roads. Hyperspectral images' classification seems to offer a solution for the detection of road material (Hong, 2020). Hyperspectral images can also be used to classify and determine the condition of roads (Mohammadi,2020). Some fusion of satellite hyperspectral images with UAV RGB images are used to detect the constituent materials of the road surface (Jenerowicz, 2017). The fusion technique is also used very successfully in other areas (Maimaitijiang, 2017). In the weather stations in the map, we can get information on the amount of precipitation in the area and thus determine the muddy, flooded, snowy, or sandy state of the soil or soil roads or contaminated or spilled with soil based on the amount of precipitation. (Kim, 2021) provides a viable solution for predicting road conditions in rainy weather using artificial neural networks. Soil properties (Ben-Dor, 2002) can also be obtained by imaging spectroscopy (Ben-Dor, 2009). All of the above provide a firm basis for the road weighting process.

Figure 1: Desired usage scenarios and the introduction diagram.

Another point worth mentioning is that for the field environment, the network connection can sometimes be poor, even if the user has downloaded a map of the area in advance. For some unavoidable reasons, such as those mentioned above, some feasible roads in the field environment are not included in the map, and the roads contained in that map are not weighted with information, so it is not possible to plan an intelligent route in real-time, but the user can provide us with the departure location and destination, and we input the two coordinate points on this map into the *A star* algorithm of (Cui, 2012) and use the weights to perform a route search. An optimal route with good road conditions can then be quickly fed back to the user. If there is no road, we can generate paths, as tracks through the terrain, estimating the "road" usability from the UAV-based scanning and searching for tracks, and the hyperspectral soil evaluation from earlier satellite data for these paths.

2 BACKGROUND

2.1 Related Dataset and Assumptions

We test our proposed approach to intelligent road route planning on the DeepGlobe Road Extraction dataset (Demir, 2018), which is publicly available and consists of 6226 training images, 1243 validation images, and 1101 test images. Each RGB image has a resolution of 1024 * 1024. Roads in this dataset are labeled as foreground and other objects are labeled as background. The imagery has 50cm pixel resolution, collected by DigitalGlobe's satellite (PGC, 2018). This also means that each picture corresponds to an actual true distance of 512 m * 512 m, and each picture covers an area of 262,144 m^2. Specific satellite information for data collection is shown in Table 1, which shows the satellite's altitude, sensor resolution, dynamic range, and other information. In Table 1, in addition to the satellite data Word-View 1 used for the collection of the above public dataset, information on Word-View 3 is shown as it provides 30cm panchromatic resolution and 1.24m multispectral resolution which can be used for pavement soil information estimation.

Table 1: DigitalGlobe Satellite (PGC, 2018).

Satellite Specifications	WorldView-1	WorldView-3
Launched:	2007	2014
Operational Altitude:	496 km	617 km
Spectral Characteristics:	Panchromatic	Panchromatic + 8 Multispectral + 8 SWIR + 12 CAVIS
Sensor Resolution:	50 cm GSD at nadir	31 cm GSD at nadir
Dynamic Range:	11-bits per pixel	11-bits per pixel, 14-bits per pixel SWIR
Swath Width:	17.7 km at nadir	13.1 km at nadir
Capacity:	1.3 million km^2	680000 km^2
per day Stereo Collection:	Yes	Yes

The dataset mentioned above was collected by satellite and, considering the practical applicability and implementation ability for real-life humans, we also tested it on an open-source dataset provided by senseFly UAV (SenseFly, 2009). This is an example dataset of a small Swiss village called Merlishachen. The imagery was collected during a single eBee Classic drone flight. The number of images in this dataset is 297, each image is (4608*3456*3), and other specific information is given in Table 2.

Table 2: eBee Classic drone dataset (SenseFly, 2009).

Technical data		
Ground resolution	Coverage	Flight height
5 cm (1.96 in)/px	0.57 sq. km (0.22 sq. mi)	162 m (531.4 ft)

The hypothetical scenarios set for this study are as follows:

- The user is in a wild and uninhabited environment, preferably after rainy or otherwise bad weather.
- Even if the user is in a place with poor or no internet connection, the user can provide the drone with its preferred starting and ending coordinates via a previously downloaded map. It can be done through a WiFi connection or by using hand gestures (Liu, 2021).
- The drone has sufficient range onboard and with a sufficiently charged battery.
- Except in the case of fog or other conditions that obstruct the drone's view.

2.2 Proposed System

The overall flow chart of this system is shown in Figure 2, the input is the real-time video sequence captured by the UAV camera, which flies at a high altitude in the sky. The captured video sequence is segmented into images by frame. The RGB image obtained is turned into a three-channel image with a resolution of 1024*1024 after image processing, at this time the data preparation work is completed. The next step is to input the processed images into *D-LinkNet* for road extraction. The extracted part of the image with the road labeled as foreground and other objects are labeled as background.

By combining this with the original RGB image and other supporting data, we weigh the extracted roads, where the main considerations are the width of the road, the connectivity of the road, and the material of the road. We mark the roads in good condition as green, meaning that the road is in better condition than the rest and that humans walk faster than the rest after rain. The rest of the roads that have not been given green priority remain white. Most of the white roads are very narrow and muddy after rainy, flooded, snowy or sandy, and are not suitable for humans to walk on. As this paper is the basis of our current research work, this section mainly presents ideas and feasible solutions, and the implementation work will be carried out in detail for the road weighting section in the future.

Finally, according to the most commonly used *A star* algorithm (Cui, 2012), we assign different values to the green and white pixel parts and use the *A star* algorithm to calculate the shortest and/or fastest path from the start point to the endpoint, to provide the best route for people in the field in any weather conditions, like being after a muddy rain.
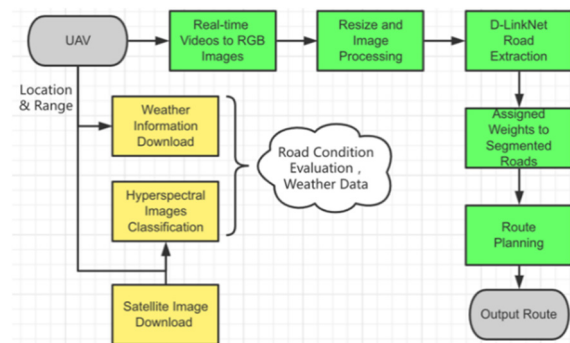

Figure 2: Flowchart of the proposed system.

3 METHODOLOGY

Figure 3 shows the key steps of this work: after the video sequence is cut into images and image processing in data preparation, the input RGB drone image is passed through *D-LinkNet*'s road extraction (Zhou, 2018) to get the extracted road-map, next the different results are shown, the right side is given the green priority road with good condition and the left side is the white normal road. For the results, the blue circles are marked with the starting point and the yellow circles with the destination, as shown by the labels on the enlarged image.
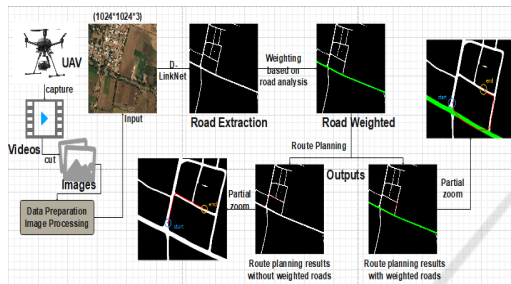

Figure 3: Key steps and comparison of results.

3.1 Data Preparation and Road Extraction Analysis

According to weather information, when bad weather has passed, which means that some roads in the field are muddy, flooded, snowy or sandy, GPU-equipped drones can capture video in real-time from high altitudes to provide route planning assistance to humans in the air below that view. The video sequence captured in real-time can be split into different images according to the frame, which is an RGB image, and then through image processing such as resize, we can get a three-channel image of the ground in the current state with a resolution of 1024*1024. This step is the data preparation stage. It lays the foundation for the subsequent road extraction and road condition analysis. The main purpose of this process is to unify, different UAVs capture images at different resolutions so the images are unified using the data processing part. For example, the images in dataset 2 will change from (4608*3456*3) to (1024*1024*3) after this process and thus enter as input into the subsequent processes of the system.

Figure 4 shows the processed RGB image input to the road extraction network. *D-LinkNet* can perform road segmentation well, labeling the roads as foreground and the others as background. The grey-scale image is combined with the original color map for road analysis, where we mainly consider the width of the road, the connectivity of the road, and the material of the road surface, because generally speaking if the road is spacious, well connected, and made of asphalt, the road will be more suitable for pedestrians or vehicles after muddy, flooded, snowy or sandy weather. Conversely, if the road is narrow, poorly connected, and composed of soil, such roads can become muddy after heavy rainfall or snowy or sandy weather. The pedestrians or drivers will find it difficult to walk or drive on them. It is therefore important to choose a road that is in good condition after the bad weather to save some time and bring convenience to humans. However, road-sections of bad conditions can also be considered if it can connect other road networks to make shortening of the path with acceptable difficulties.

Figure 4: Road extraction, analysis, and marking of green priority roads.

It is important to note here that the *D-LinkNet* segmentation does not reach 100%, so there is a difference between the results of the road extraction and the real situation of the original image. For road material detection, researchers (Hong, 2020) have been able to identify asphalt and soil based on hyperspectral image segmentation techniques, although the two tasks are based on different data sets. Hyperspectral images can also be used to classify and determine the condition of roads (Mohammadi, 2020). Last but not least, weather information is also important and we can get relevant real-time and past period weather information from the radar. The weather information was downloaded by the scouting UAV before starting into the wild. It can provide the amount of precipitation in the area, and there are precipitation values whose magnitude directly affects the road conditions of the material is soil, so this information coupled with the fusion of hyperspectral imagery with drone imagery will be added to our research work in the future. By combining these elements, we can assign weights to the roads extracted from the map in a very comprehensive way. And now we compare only the original RGB image with the segmented road grey image, which is given priority based on the two factors of road connectivity and width and is labeled as a green road, the rest remaining white.

3.2 *A Star* Algorithm and Weighted Route Planning

The *A-star* algorithm (Cui, 2012) is a heuristic search algorithm for global path planning. It has been successfully implemented and tested as a path planning algorithm for mobile robots. The results can be found in (Kuswadi, 2018). This algorithm uses a combination of heuristic searching and searching based on the shortest path. It is defined as the best-first algorithm because each cell in the configuration space is evaluated by the value:

$$f(n) = h(n) + g(n) \qquad (1)$$

where *g(n)* represents the cost from the starting point to the current node; *h(n)* represents the estimated cost from the current node to the ending point; *n* is the current node.

The definition of a white node is a no-priority road and the green node is the road with priority. Figure 5 shows the assignment of values for *g(n)* in different pixel cases when the node is surrounded by white pixels, which means the node without priority and be accessible, then the point is the top and bottom left and right nodes are each assigned a value of 100, the diagonal length of the four points in the diagonal direction of the node is 140. The other case, when the node is surrounded by green pixel points, that is, with priority access to the road, then the corresponding value is reduced by a factor of 100, again when both are present as shown in Figure 5, the algorithm gives preference to the green node with a small loss value since the minimum *f- value* is to be obtained. In Figure 5, the leftmost plot shows that the pixel is on a road that is not given priority and that the pixel is surrounded by non-priority roads, the middle plot shows that the pixel is on a road that is given priority and that it is surrounded by pixels that are given priority, and the rightmost plot shows a critical state where the intersection of the two, the road that is given priority and the road that is not given priority We randomly select the top right two pixel points to be labelled as priority roads and the rest as non-priority roads, then the algorithm comes into play, and this is where the assignment of values at the pixel level in the *g(n)* function comes into play.

Figure 5: Different assignment of *g(n)* cost value to different pixel points.

There are several well-known heuristic mathematical functions *h(n)* that can be used (Heuristics, 2019), the most commonly used are Euclidean distance h_E, Manhattan distance h_M, or Diagonal distance h_D. In this work, we have chosen to use the h_D to calculate the diagonal distance with the weighted modification:

$$dx = |x_n - x_g| \qquad (2)$$

$$dy = |y_n - y_g| \qquad (3)$$

$$h_E(n) = \sqrt{dx^2 + dy^2} \qquad (4)$$

$$h_M(n) = dx + dy \qquad (5)$$

$$h_D(n) = d_1 * max(dx, dy) + (d_2 - d_1) \qquad (6)$$
$$* min(dx, dy)$$

Where (x_n, y_n) is the coordinate of the current node *n*; (x_g, y_g) is the coordinate of the end node *n*; For green cell d_1=1 and d_2=1.4 (octile distance), white cell d_1=100 and d_2=140.

Put the 8 adjacent nodes of the starting point into the open list and if the adjacent node is unreachable, then remove this node from the open list. Using Equation (1) to calculate the cost function formula for the adjacent nodes, the one with the smallest *f-value* is chosen as the next node and the previous nodes are put into the closed list. The sequence continues until the current node is the end position, and finally, a path with the smallest *f-value* from the start to the end will be found, which is the optimal path.

4 EXPERIMENTS

We tested the main part of this work on the publicly available DeepGlobe Road Extraction dataset (Demir, 2018) and SenseFly dataset (SenseFly, 2009). We also evaluated the time required for each phase of this work. Three sets of experiments were carried out in the DeepGlobe Road Extraction dataset and the results can be found in Table 3 the three tests are shown in Figure 6, Figure 7, and Figure 8. In these figures, blue circles indicate the starting point, yellow circles indicate the destination and the route is in red. The route is pixel level, so we have intercepted a portion of the map to zoom in on the results. For better presentation, we have deepened the route color by also labeling the 8 neighboring points near each pixel of the route as red.

In the data preparation phase, the time required for this part of the conversion of the live video sequence

captured by the UAV onboard camera into the input image needed for the road extraction part is directly related to the duration of the video sequence, in general for a video with a duration of 17 seconds, the real-time time required for data processing is 1.25 seconds, and the time required for road extraction by *D-LinkNet* is about 5 seconds, followed by the assignment of road priority, which will be extended to be done automatically in the future, based on the research of other researchers (Hong, 2020). We were able to extract the two indices they had classified well, namely asphalt and soil in the Pavia University data set (Zhu, 2021), and assign road priority based on the results of the road material classification and road conditions. We also combine weather information and soil information from the fusion of satellite and drone imagery to carry out automatic road weighting. The time required for the final route planning is around 20 seconds, which is related to the location of the starting point and ending point.

Table 3: Testing results on the DeepGlobe Road Extraction dataset.

Table Head	Comparison		
	Starting point	Ending point	f -value
Fig 6 (left)	(663,673)	(975,445)	36110
Fig 6 (right)	(663,673)	(975,445)	24436
Fig 7 (left)	(719,545)	(566,127)	4733
Fig 7 (right)	(719,545)	(566,127)	1004
Fig 8 (left)	(450,440)	(890,264)	36230
Fig 8 (right)	(450,440)	(890,264)	36230

In Figure 6, the starting point is at (663, 673) and the ending point is at (975, 445). For the graph without priority road assignment, the final *f-value* from the starting point to the ending point is 36110 based on the *A star* algorithm, noting that the value of *f* here only represents the cost value calculated under a specific parameter setting and does not represent the real length of the route, which is positively correlated with each other. The relationship between them is positive. On the right-hand side of Figure 6, when the map has green roads, i.e. roads with priority, it is clear that the route length increases, but the *f-value* decreases, with a value of 24,436 and 32.3% less than on the left-hand side. A smaller *f-value* means that the user can reach the destination faster.
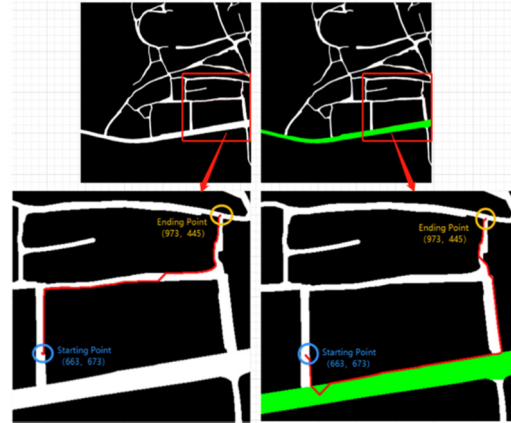

Figure 6: Test result 1 on the DeepGlobe Road Extraction dataset (The right half comes with road priority, while the left half does not).

Figure 7 shows the same experiment in another map with the coordinates of (719,545) for the starting location and (566,127) for the ending location. The range of this experiment is smaller compared to that of test 1 in Figure 6, which means that the place the user needs to go is not very far away, it is nearby. From the results in Figure 7, the *f-value* without road priority is 4733 and the *f-value* with road priority is 1044, which is 78% lower than the former, which largely helps the user to choose the best route.
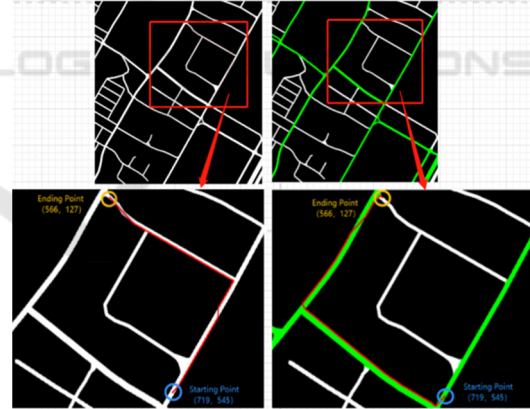

Figure 7: Test result 2 on the DeepGlobe Road Extraction dataset (The right half comes with road priority, while the left half does not.).

Figure 8 shows another representative aspect of the experiment, when the destination that the user wants to go to and the priority path that can be resorted to are in opposite directions, the results of the experiment also show that the path with priority does not come into play at this point, i.e. the two results are the same, and from Figure 8 we can see that the coordinates of the position of the starting point are

(450,440). The position coordinates of the endpoint are (890,264) and the value of f is the same in both cases. Similarly, if the user is on a road in poor condition, but his or her destination is close, or even insight, then the user will certainly not take a detour to a road in good condition to reach his or her destination. The final decision depends on the smallest *f-value*.
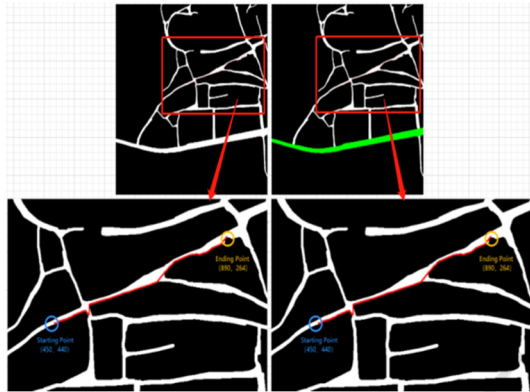

Figure 8: Test result 3 on the DeepGlobe Road Extraction dataset (The right half comes with road priority, while the left half does not).

As the main application of this system is for UAVs rather than satellites, we also tested it in dataset 2, and the results obtained are shown in Figure 9 and Figure 10. Figure 9 illustrates the change in the size of the drone image from (4608*3456*3) to (1024*1024*3) after basic image processing. After *D-LinkNe*t 's road extraction the greyscale image containing the roads is obtained and finally, the weighting of the roads is assigned. As the data images collected for this dataset are small villages, in this image unlike the satellite image above, where asphalt roads are predominant, most of the roads are given priority. The actual application environment is a sparsely populated wilderness where the roads are not in such good condition and the area covered is larger than this.
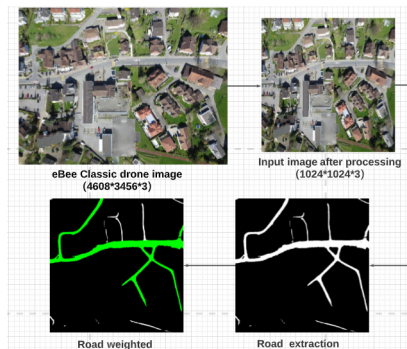

Figure 9: Test result on eBee Classic drone dataset.

Figure 10 shows the results of route planning, where the coordinates of the starting point are (718,190) and the coordinates of the ending point are (288,420). The left half represents the real-time route planned when the road is not given priority, and the final *f-value* obtained is 45250. In contrast, the right half of Figure 12 shows the route planned for the green road given priority, and the *f-value* obtained in this case is 560, which shows that there is an improvement of 98%.
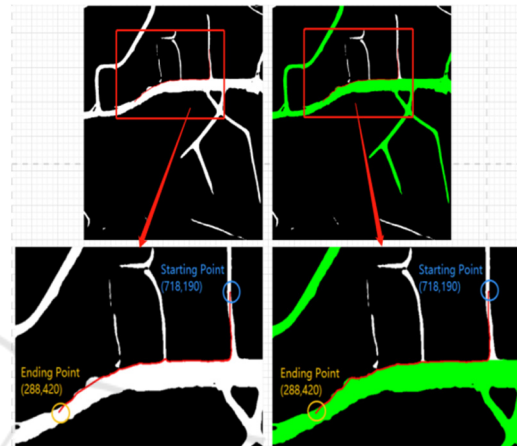

Figure 10: Test result on eBee Classic drone dataset (route planning).

5 DISCUSSION AND CONCLUSION

This paper focuses on a project to provide users with optimal route planning based on the latest road extraction techniques, which are of interest in the field after heavy rain or the strong snowing, or heavy sandstorm contaminating the road surface. The satellite hyperspectral info can address the information of road conditions as the close neighborhood soil, vegetation hiding, 3D info for floods. Drones offer a great deal of flexibility, and GPU-equipped drones can fly in the field in real-time to provide some assistance to users in that environment by WiFi or human gesture recognition. The images captured by the UAV also have a high resolution, and drone communicates more easily with people than satellites. In this paper, we have tested both on publicly available satellite images and on smaller publicly available UAV images, both of which achieved the desired results. The first step in this work is to segment the live video sequence captured by the UAV into a fixed pixel RGB three-channel image. The next step is to input this map

image into *D-LinkNet* for road extraction, resulting in a grey image with white-labeled as the road and the rest black as the background. Finally, the roads are given weight after some road analysis, where the road information refers to the width, connectivity, and road surface material. Roads with green pixels have priority. The *A star* algorithm was used for route planning and the results were compared between the map image with priority roads and the map image without priority roads.

This work also has some limitations due to the presence of many assumptions in this work. For example, the environment to which this work applies would ideally be in the wild and after bad weather, when some roads in the wild are in a very muddy, flooded, snowy or sandy state unsuitable for human walking. Next, we need to automate this part of the road weighting process. Based on the weather information provided by the weather stations on the map, the amount of precipitation can be further assessed. The value of precipitation directly affects the road condition of a soil road in a field environment, which is one of the factors to be considered. Secondly, according to the mature hyperspectral classification technology, we can choose to fuse hyperspectral images of satellites and recent UAV RGB images to extract the index of asphalt and soil, which is the second point of the basis for weighting, and finally, we can integrate the length and width information of the segmented road to achieve the automated road weighting. In the future, a comparative analysis of the impact of different $h(n)$ functions on route planning will also be carried out, as well as some improvements to the algorithm. In the end, we also need to test this in the real world with GPU-equipped drones rather than on publicly available datasets.

ACKNOWLEDGMENTS

REFERENCES

Apolo-Apolo, O. E., J. Martínez-Guanter, G. Egea, P. Raja, and M. Pérez-Ruiz. (2020)"Deep learning techniques for estimation of the yield and size of citrus fruits using a UAV." European Journal of Agronomy 115 126030.

Ghelichi, Zabih, Monica Gentili, and Pitu B. Mirchandani. (2021) "Logistics for a fleet of drones for medical item delivery: A case study for Louisville, KY." Computers & Operations Research 135 105443.

Moumgiakmas, Seraphim S., Gerasimos G. Samatas, and George A. Papakostas. (2021) "Computer vision for fire detection on UAVs—From software to hardware." Future Internet 13, no. 8 200.

Rizk, Hamada, Yukako Nishimur, Hirozumi Yamaguchi, and Teruo Higashino. (2022) "Drone-Based Water Level Detection in Flood Disasters." International Journal of Environmental Research and Public Health 19, no. 1 237.

Galkin, Boris, Jacek Kibilda, and Luiz A. DaSilva. (2019) "UAVs as mobile infrastructure: Addressing battery lifetime." IEEE Communications Magazine 57, no. 6 132-137.

Ciepłuch, Błażej, Ricky Jacob, Peter Mooney, and Adam C. Winstanley.(2010) "Comparison of the accuracy of OpenStreetMap for Ireland with Google Maps and Bing Maps." In Proceedings of the Ninth International Symposium on Spatial Accuracy Assessment in Natural Resuorces and Enviromental Sciences 20-23rd July 2010, p. 337. University of Leicester, 2010.

Liu, Chang, and Tamás Szirányi. (2021) "Real-Time Human Detection and Gesture Recognition for On-Board UAV Rescue." Sensors 21, no. 6 2180.

Zhou, Lichen, Chuang Zhang, and Ming Wu. (2018) "D-linknet: Linknet with pretrained encoder and dilated convolution for high resolution satellite imagery road extraction." In Proceedings of the IEEE Conference on Computer Vision and Pattern Recognition Workshops, pp. 182-186.

Hong, Danfeng, Lianru Gao, Jing Yao, Bing Zhang, Antonio Plaza, and Jocelyn Chanussot. (2020) "Graph convolutional networks for hyperspectral image classification." IEEE Transactions on Geoscience and Remote Sensing.

Mohammadi, M. (2012) "Road classification and condition determination using hyperspectral imagery." Int. Arch. Photogramm. Remote Sens. Spatial Inf. Sci 39 B7.

Jenerowicz, Agnieszka, Katarzyna Siok, Malgorzata Woroszkiewicz, and Agata Orych. (2017) "The fusion of satellite and UAV data: simulation of high spatial resolution band." In Remote Sensing for Agriculture, Ecosystems, and Hydrology XIX, vol. 10421, p. 104211Z. International Society for Optics and Photonics.

Maimaitijiang, Maitiniyazi, Vasit Sagan, Paheding Sidike, Ahmad M. Daloye, Hasanjan Erkbol, and Felix B. Fritschi. (2020) "Crop Monitoring Using Satellite/UAV Data Fusion and Machine Learning." Remote Sensing 12, no. 9 1357.

Kim, Sangyoup, Jonghak Lee, and Taekwan Yoon. (2021) "Road surface conditions forecasting in rainy weather using artificial neural networks." Safety science 140 105302.

Ben-Dor, E. (2002) "Quantitative remote sensing of soil properties." 173-243.

Ben-Dor, E., Sabine Chabrillat, J. Al M. Demattê, G. R. Taylor, J. Hill, M. L. Whiting, and S. Sommer. (2009) "Using imaging spectroscopy to study soil properties." Remote sensing of environment 113 S38-S55.

Cui, Shi-Gang, Hui Wang, and Li Yang. (2012) "A simulation study of A-star algorithm for robot path planning." In 16th international conference on mechatronics technology, pp. 506-510.

Demir, Ilke, Krzysztof Koperski, David Lindenbaum, Guan Pang, Jing Huang, Saikat Basu, Forest Hughes, Devis Tuia, and Ramesh Raskar. (2018) "Deepglobe 2018: A challenge to parse the earth through satellite images." In Proceedings of the IEEE Conference on Computer Vision and Pattern Recognition Workshops, pp. 172-181.

PGC. "DigitalGlobe Satellite Constellation – Polar Geospatial Center." Www.pgc.umn.edu, 20 Mar. 2018, www.pgc.umn.edu/guides/commercial-imagery/digitalglobe-satellite-constellation/. Accessed 27 Jan. 2022.

"Discover a Wide Range of Drone Datasets." SenseFly, www.sensefly.com/education/datasets/?dataset=1419 &sensors%5B%5D=24. Accessed 25 Jan. 2022.

Kuswadi, Son, Jeffri Wahyu Santoso, M. Nasyir Tamara, and Mohammad Nuh. (2018) "Application SLAM and path planning using A-star algorithm for mobile robot in indoor disaster area." In 2018 International Electronics Symposium on Engineering Technology and Applications (IES-ETA), pp. 270-274. IEEE.

"Heuristics." Stanford.edu, 2019, theory.stanford.edu/~amitp/GameProgramming/Heuristics.html.

Zhu, Qiqi, Weihuan Deng, Zhuo Zheng, Yanfei Zhong, Qingfeng Guan, Weihua Lin, Liangpei Zhang, and Deren Li. (2021) "A Spectral-Spatial-Dependent Global Learning Framework for Insufficient and Imbalanced Hyperspectral Image Classification." IEEE Transactions on Cybernetics.